Crystal structures of the NAD$^+$-reducing soluble [NiFe]-hydrogenase

Hydrogenases catalyze the synthesis and decomposition of molecular hydrogen ($2H^+ + 2e^- \leftrightarrow H_2$). The enzymes are classified into three types based on the metal composition of the active site: Ni–Fe, Fe–Fe, and Fe types. Of these, [NiFe]-hydrogenases comprise the widest variety of members regarding their physiological function, whereas the hydrogenase unit, consisting of large and small subunits, is highly conserved among the members, and the peripheral unit and cellular localization mainly determine their functions. It has been proposed that the physiological function of the NAD$^+$-reducing soluble [NiFe]-hydrogenase (SH), a member of the group III [NiFe]-hydrogenase, is the consumption of the excess amount of reducing equivalents by coupling the oxidation of NADH and the synthesis of H_2 (Fig. 1(a)) [1]. While SH from some organisms contains auxiliary subunit(s), the core of the enzyme complex is conserved as a heterotetrameric complex consisting of the diaphorase unit (HoxFU subcomplex) and hydrogenase unit (HoxYH subcomplex). Amino acid sequence analyses have indicated that the four subunits are evolutionally related to those of NADH:quinone oxidoreductase (complex I), which is responsible for the first step of the respiratory chain by coupling the oxidation of NADH and the reduction of quinone species (Fig. 1(b)) [2]. As with complex I, SH functions in organisms that grow under oxic environments. It has been widely accepted that the active sites of the hydrogenases are highly sensitive to O_2 and that some mechanism is required to protect SH from O_2 attack. In order to obtain insights into the O_2 protection mechanism and molecular evolutional relationship between SH and complex I, we have determined the X-ray crystal structures of SH [3].

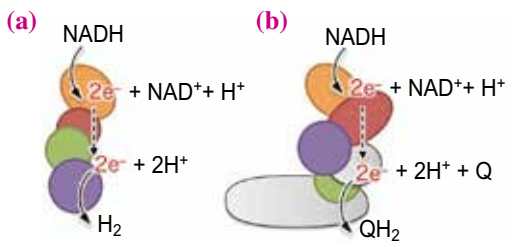

Fig. 1. Physiological reactions catalyzed by SH **(a)** and complex I **(b)**. "Q" represents quinone species. Homologous subunits are shown in the same color. It has been proposed that complex I mechanically couples the quinone reduction and proton pumping, which is omitted in (b).

SH was extracted and purified from *Hydrogenophilus thermoluteolus* TH-1, a thermophilic H_2-oxidizing bacterium, without any genetic manipulation [4]. The purification and crystallization were performed under aerobic conditions, and the crystals of the as-purified sample were termed the air-oxidized state and those soaked in a buffer containing 1 mM benzyl viologen (BV) and saturated H_2 at 0.1 MPa for 24 h at 293 K were termed the H_2-reduced state. During the soaking, the reduction of BV and the oxidation of H_2 by SH occurred, as indicated by the blue color of the reduced BV around the crystals. X-ray diffraction experiments were performed at SPring-8 beamlines **BL32XU**, **BL38B1**, **BL41XU**, and **BL44XU**. The final sets of data of the air-oxidized and H_2-reduced states were collected at BL44XU. The initial phases were calculated using single anomalous dispersion signals from the intrinsic iron and nickel atoms in SH, and the structure models for the air-oxidized and H_2-reduced states were refined to 2.58 and 2.70 Å resolution, respectively.

The overall structure shows a heterotetrameric architecture (Fig. 2(a)) consisting of the diaphorase HoxFU (~90 kDa) and hydrogenase HoxHY (~73 kDa) subcomplexes, sharing a shape-complementary interaction with an interface area of 2084 Å^2, which shares 4.4% of the total surface of the heterotetramer. As predicted from the amino acid sequence analyses [2], each subunit has a structural similarity to that of complex I. HoxF (residues 165–438), HoxU, HoxY, and HoxH are superposed on Nqo1, Nqo3, Nqo6, and Nqo4 of complex I from *Thermus thermophilus* HB8 (*Tt*-complex I) [5] with root mean square deviation (r.m.s.d.) values of 1.6, 2.1, 2.6, and 2.3 Å for 256, 174, 83, and 228 Cα atoms, respectively. In addition, the N-terminal part of HoxF (9–127) is superposed on Nqo2 with an r.m.s.d. of 1.8 Å for 115 Cα residues, revealing that HoxF has evolved as a fusion protein of Nqo1 and Nqo2. In contrast to the structural similarities between SH and complex I at the tertiary structure level, the superposition of the tetrameric SH complex on complex I requires a considerable rigid body movement of either subcomplex (Figs. 2(a) and 2(b)). Superposition of the Nqo1•2•3 subcomplex of *Tt*-complex I on the HoxFU subcomplex of SH revealed that the species of Fe–S clusters and their positions are highly conserved except for N1a [2Fe–2S] and N7 [4Fe–4S] clusters, which are inherently absent in SH and located at off-line positions of the electron-transfer pathway in *Tt*-complex I, implying

that SH has a minimum set of Fe–S clusters for the electron transfer. The different orientations of subcomplexes supports the hypothesis that the hydrogenase and Nqo4•6 subcomplexes diverged at some point of the molecular evolutional process and independently acquired the diaphorase subcomplex, which was assembled into each energy metabolism machinery.

One of the most prominent structural differences between air-oxidized and H_2-reduced states was observed at the Ni–Fe active site. The coordination geometry of the Ni–Fe cluster of the air-oxidized state with no precedent in nature showed that the carboxy group of Glu32 binds six-coordinate Ni as a bidentate ligand (Fig. 3), which is in contrast to the previously reported Ni–Fe clusters consisting of five-coordinate Ni without binding of the carboxy group. On the other hand, the Ni–Fe active site of the H_2-reduced state has a regular coordination geometry (Fig. 3). Electron paramagnetic resonance spectroscopic analyses detected signals of the oxidized state attributable to Ni(III) that do not match those identified for the oxidized states of [NiFe]-hydrogenases, implying that the distinct configuration of the Ni–Fe active site of the oxidized SH is not an artifact caused by the crystallization or X-ray exposure during the diffraction data collection. On the basis of the structure comparison between the air-oxidized and H_2-reduced states, we assume that the redox-dependent conformational change is induced by the reduction and oxidation of the proximal Y1 [4Fe–4S] cluster. When the Y1 cluster maintains the oxidized $[4Fe–4S]^{2+}$ state for a certain time period, the guanidinium group of Arg58 moves away from the Fe–S cluster owing to electrostatic repulsion. The displacement of Arg58 is transferred to Glu32 via the hydrogen-bond network, resulting in the coordination of Glu32 to Ni (Fig. 3). The Ni–Fe active site in the air-oxidized form appears to be highly resistant against O_2 attack because of the formation of the six-coordinate Ni complex. This finding suggests that the proximal Fe–S cluster functions not only as a component of the electron-transfer pathway but also as an oxidative stress sensor to protect the Ni–Fe active site from O_2.

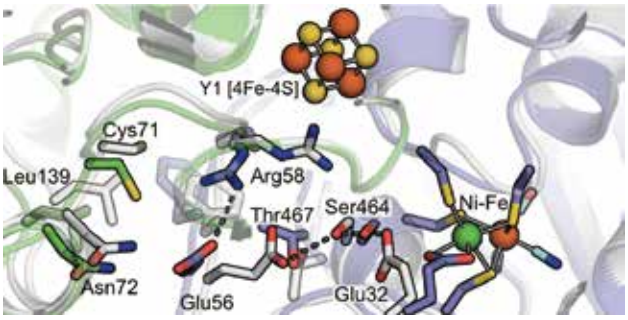

Fig. 3. Structure comparison of SH in the air-oxidized and H_2-reduced states. The air-oxidized state is shown in the same colors as in Fig. 2, and the H_2-reduced state is shown in white. For clarity, the Ni–Fe active site and Y1 cluster are shown only for the air-oxidized state.

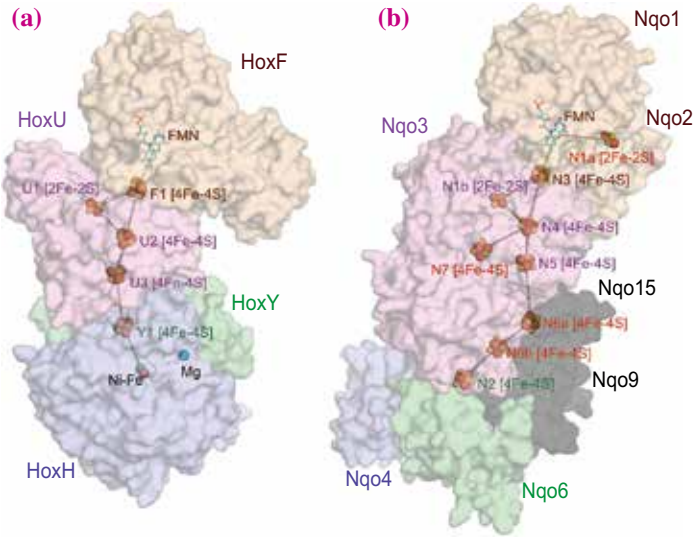

Fig. 2. Structure comparison of SH **(a)** and soluble part of *Tt*-complex I **(b)**. Surface representations of the protein molecules and sphere/stick models of the redox centers are shown. Homologous subunits are represented in the same color. The Fe–S clusters in red characters in (b) are not found in SH.

Yasuhito Shomura[a,*] and Yoshiki Higuchi[b,c]

[a] Institute of Quantum Beam Science, Ibaraki University
[b] Department of Picobiology, University of Hyogo
[c] JST/CREST

*Email: yasuhito.shomura.s@vc.ibaraki.ac.jp

References

[1] K. Schneider *et al.*: Biochim. Biophys. Acta - Enzymol. **452** (1976) 66.
[2] R. Böhm *et al.*: Mol. Microbiol. **4** (1990) 231.
[3] *Y. Shomura, M. Taketa, H. Nakashima, H. Tai, H. Nakagawa, Y. Ikeda, M. Ishii, Y. Igarashi, H. Nishihara, K-S. Yoon, S. Ogo, S. Hirota, Y. Higuchi: Science* ***357*** *(2017) 928.*
[4] M. Taketa *et al.*: Acta Crystallog. Sect. F **71** (2015) 96.
[5] R. Baradaran *et al.*: Nature **494** (2013) 443.